PROCEEDINGS OF SPIE

SPIEDigitalLibrary.org/conference-proceedings-of-spie

Improved misfit function for attenuation and speed reconstruction in ultrasound computed tomography

M. Pérez-Liva, J. M. Udías, J. L. Herraiz

M. Pérez-Liva, J. M. Udías, J. L. Herraiz, "Improved misfit function for attenuation and speed reconstruction in ultrasound computed tomography," Proc. SPIE 10139, Medical Imaging 2017: Ultrasonic Imaging and Tomography, 101390O (13 March 2017); doi: 10.1117/12.2253849

SPIE.

Event: SPIE Medical Imaging, 2017, Orlando, Florida, United States

Downloaded From: https://www.spiedigitallibrary.org/conference-proceedings-of-spie on 11/27/2017 Terms of Use: https://www.spiedigitallibrary.org/terms-of-use

Improved misfit function for attenuation and speed reconstruction in ultrasound computed tomography

M. Pérez-Liva*[a], J.M Udías[a], J.L Herraiz[a]
[a]Grupo de Física Nuclear, Dpto. de Física Atómica, Molecular y Nuclear, Universidad Complutense de Madrid, CEI Moncloa, Av. Complutense S/N, Facultad de C.C. Físicas, Madrid 28040, Spain

ABSTRACT

The reconstruction of acoustic attenuation maps for transmission Ultrasound Computed Tomography (USCT) based on the standard least-squares full wave inversion method requires the accurate knowledge of the sound speed map in the region under study. Any deviation in the reconstructed speed maps creates a very significant bias in the attenuation map, as the standard least-squares misfit function is more sensitive to time misalignments than to amplitude differences of the signals. In this work, we propose a generalized misfit function which includes an additional term that accounts for the amplitude differences between the measured and the estimated signals. The functional gradients used to minimize the proposed misfit function were obtained using an adjoint field formulation and the fractional Laplacian wave equation. The forward and backward wave propagation was obtained with the parallelized GPU version of the software k-Wave and the optimization was performed with a line search method. A numerical phantom simulating breast tissue and synthetic noisy data were used to test the performance of the proposed misfit function. The attenuation was reconstructed based on a converged speed map. An edge-preserving regularization method based on total variation was also implemented. To quantify the quality of the results, the mean values and their standard deviations in several regions of interest were analyzed and compared to the reference values. The proposed generalized misfit function decreases considerably the bias in the attenuation map caused by the deviations in the speed map in all the regions of interest analyzed.

Keywords: Generalized misfit function, full wave inversion, sound speed and attenuation reconstruction, time domain.

1. INTRODUCTION

Ultrasound computed tomography (USCT) is a non-invasive radiation-free medical imaging technique with increasing application for breast cancer studies. This technique allows reconstructing several acoustical properties of the tissue like the sound speed (SS) and the acoustic attenuation (AA). The SS in a particular tissue correlates well with its density[1], and therefore, its measurement has been proposed for breast cancer detection, as it may yield images with similar levels of contrast to those obtained from X-ray mammograms. USCT can also provide information of the AA coefficient, which depends on the tissue type much more than the density and the SS, and it holds the potential to improve significantly the detectability of malignancies in the body[1].

Full-wave inversion (FWI) algorithms achieve USCT images with high spatial resolution by solving the full wave equation that describes the propagation of the ultrasound waves in the tissues. The basis of FWI methods were laid out by Tarantola[2] in the field of seismology, where he introduced the formalism of the minimization of the least squares functional comprised by the waveform differences between observed and simulated waveforms by iterative gradient methods. The reconstruction of SS maps with FWI has been widely studied and it has been quite demonstrated the robustness of the method to provide high-resolution SS images[3-5]. Nevertheless, with the current formulations, the reconstruction of the AA maps is more challenging than the reconstruction of SS maps. This is because the standard least squares misfit function is more sensitive to variations of the SS than of the AA. This means that if the SS map is not perfectly estimated, the reconstructed AA map will be significantly biased [6,7].

*mailyn01@ucm.es phone: +34 913944484

Medical Imaging 2017: Ultrasonic Imaging and Tomography, edited by Neb Duric, Brecht Heyde, Proc. of SPIE Vol. 10139, 101390O · © 2017 SPIE · CCC code: 1605-7422/17/$18 · doi: 10.1117/12.2253849

Downloaded From: https://www.spiedigitallibrary.org/conference-proceedings-of-spie on 11/27/2017 Terms of Use: https://www.spiedigitallibrary.org/terms-of-use

Many different misfit functions for FWI have been proposed[8,9] in order to remark different aspects of the ultrasonic wavefield. The ones based only on travel-time or amplitude differences are robust as initial estimations in an iterative reconstruction. Moreover, these approaches are also useful as a way to reduce the high non-linearity that FWI methods suffer and also to isolate the influence of a single acoustic property in the measured signals. Nevertheless, these error functionals yield poor resolution images due to the fact that the same time independent correction is applied along the entire kernel that relates an emitter-receiver pair, known as banana-doughnut kernels[10]. On the other hand, the standard least squares misfit function provides high resolution images, but it may fail if the error functional can be affected by more than one material property, especially if the initial estimations of these properties are slightly far from the actual values. This is what happens when using the least squares functional to update the AA distribution. Due to that, we propose a misfit function that includes an extra term that combines the effect of the standard least squares misfit with the amplitude differences between the signals due to AA. This combination facilitates the convergence of reconstruction of the AA map and makes the reconstruction process more independent on the possible errors in the estimated SS map.

2. METHODS

2.1 Forward problem

We consider a lossy medium in which the acoustic absorption follows a frequency power law of the form $\alpha = \alpha_0 \omega^y$, where α_0 is the absorption proportionality coefficient in Np (rad/s)$^{-y}$ m^{-1}, ω is the time frequency in rad/s, and y is the power law exponent (in this work, this is assumed to be constant and equal to 1.5[11]). The propagation of acoustic waves in this medium can be described by the fractional Laplacian wave equation[12,13]

$$\left[\frac{1}{c^2}\frac{\partial^2}{\partial t^2} - \nabla^2 - \tau_1(-\nabla^2)^{\frac{y}{2}}\frac{\partial}{\partial t} - \tau_2(-\nabla^2)^{\frac{y+1}{2}}\right] p(\boldsymbol{r}, t) = S(\boldsymbol{r}, t). \quad (1)$$

Here $p(\boldsymbol{r}, t)$ is the acoustic pressure as function of spatial position $\boldsymbol{r}$ and time t, S is a source term, c is the SS. The terms in τ_1 and τ_2 account for acoustic absorption and dispersion respectively, and are given by:

$$\tau_1 = -2\alpha_0 c^{y-1}, \tau_2 = 2\alpha_0 c^y \tan\left(\frac{\pi y}{2}\right). \quad (2)$$

To solve the fractional Laplacian wave equation, we employed a parallelized GPU version of the open-source k-Wave toolbox written in C++ and CUDA[14,15] which solves an equivalent system of coupled first-order partial differential equations based on the conservation of mass, momentum, and energy in the given medium. This code uses the k-space pseudo-spectral method to discretize the governing equations, which allows accurate simulations close to the Nyquist limit of two grid points per wavelength.

2.2 Inverse problem

The FWI methods are based on the minimization of a chosen cost function employing iterative gradient algorithms. The commonly used least squares misfit function is obtained the sum of the squares of the differences between experimental p^{obs} and simulated signals p:

$$\varepsilon = \frac{1}{2}\sum_{m=1}^{M}\int_o^T [p(\boldsymbol{r}_m) - p^{obs}(\boldsymbol{r}_m)]^2\, dt + \mu R_{TV}\,. \quad (3)$$

Here m represents each of the M emitters considered, μ controls the relative importance of the total variation (TV) regularization term given by the functional R_{TV}[16].

$$R_{TV} = \sum_{i,j}\sqrt{\xi_{x,i,j}^2 + \xi_{y,i,j}^2 + \theta}\,. \quad (4)$$

In Eq. (4), $\xi_{x,i,j}$ and $\xi_{y,i,j}$ are the derivatives of the acoustical property ξ with respect to x and y, respectively, at the pixel (i, j). The parameter θ ensures that R_{TV} is continuously differentiable.

Downloaded From: https://www.spiedigitallibrary.org/conference-proceedings-of-spie on 11/27/2017 Terms of Use: https://www.spiedigitallibrary.org/terms-of-use

The cost function we propose in this work to make the reconstruction of the AA distribution more robust against possible deviations from the real SS model is given by:

$$\varepsilon' = \frac{1}{2}\sum_{m=1}^{M}\int_o^T [p(\boldsymbol{r_m}) - p^{obs}(\boldsymbol{r_m})]^2\, dt \; + \beta\frac{1}{2}\sum_{m=1}^{M}\left(\frac{{A_m}^{obs}}{A_m} - 1\right)^2 + \mu R_{TV} \tag{5}$$

Here ${A_m}^{obs}$ and A_m are the amplitudes of the observed and predicted waveforms at the receivers position.

To illustrate the features of the proposed misfit we present a numerical example. We calculated the functional errors ε and ε' for pulses delayed in time and modified in amplitude with respect to a reference signal that presents a fixed value of amplitude and time delay. This process is equivalent to consider continuous modifications in the SS and AA in a homogenous region of the medium. The results are shown in Fig. 1:

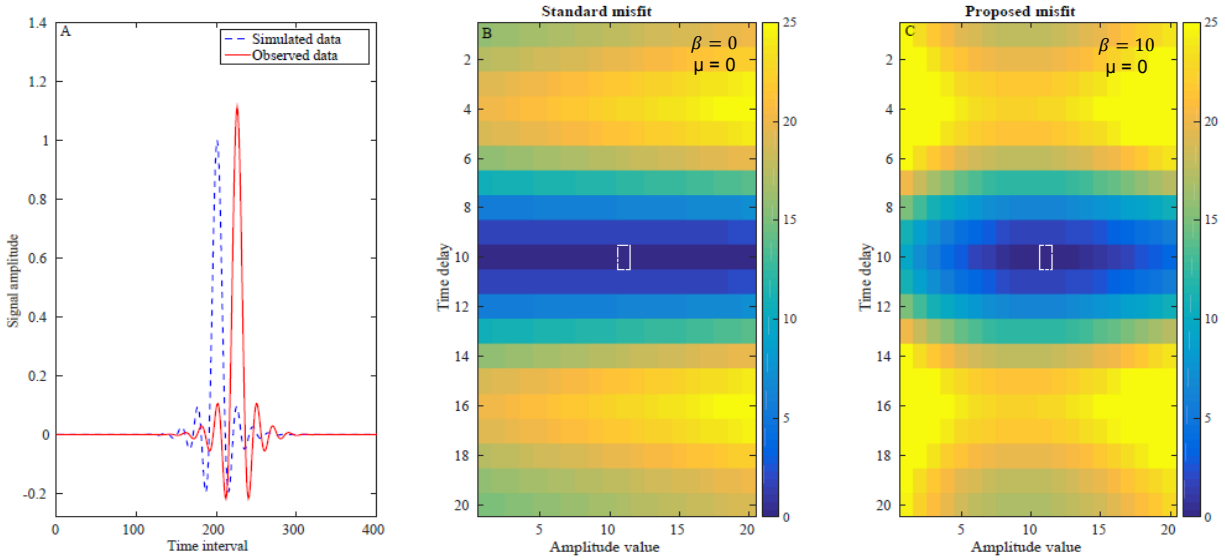

Figure. 1. A. Example of simulated signals used to calculate the global error behavior with different misfit functions. The simulated signal (in dashed blue line) is displaced around the reference time of flight value (in red) and its amplitude is modified around the reference value as well. B. Result obtained with the standard squares misfit function. C. Results obtained with the proposed misfit function. Minimum values were squared with dashed white line.

As Fig. 1 B illustrates, when using the standard misfit function ε, it is crucial to have an initial estimate of the SS very close to the real one in order to update the AA distribution. In the horizontal axis this distribution is only convex at the exact reference value of time delay (i.e. at the reference SS). On the other hand, the proposed error functional ε' does not require accounting with the exact value of SS to reach the actual minimum of ε' with respect to the AA (see Fig. 1 C.). The problem is more convex in all the directions. Fig. 1 also demonstrates that the SS could be recovered from a fairly arbitrary initial model for the AA.

To reconstruct both SS and AA distribution we used an alternating minimization scheme[17] as the error functional ε' (Eq. 5) depends on both c and α_0. This method allows dividing the optimization problem into two sub-problems, one in which c is estimated for a fixed α_0 and another in which α_0 is estimated for a fixed c:

$$c^{n+1}(\boldsymbol{r}) = c^n(\boldsymbol{r}) + {\lambda_c}^n \frac{\partial \varepsilon^n}{\partial c}\,. \tag{6}$$

$${\alpha_0}^{n+1}(\boldsymbol{r}) = {\alpha_0}^n(\boldsymbol{r}) + {\lambda_{\alpha_0}}^n \frac{\partial \varepsilon^{\,n}}{\partial \alpha_0}\,. \tag{7}$$

Downloaded From: https://www.spiedigitallibrary.org/conference-proceedings-of-spie on 11/27/2017 Terms of Use: https://www.spiedigitallibrary.org/terms-of-use

Here λ^n is the step size for the n^{th} iteration, which in this work is calculated using a line-search method[18]. To obtain the functional gradients $\frac{\partial \varepsilon}{\partial \alpha_0}$ and $\frac{\partial \varepsilon}{\partial c}$ we employed an adjoint method[19] and derived the gradient expression based[7,23] using the fractional Laplacian wave equation (Eq. 1)

$$\frac{\partial \varepsilon}{\partial c} \approx \sum_{m=1}^{M} \int_0^T p^*(\mathbf{r}, T-t)\, w(T-t)\, \frac{2}{c^3}\left(\frac{\partial^2}{\partial t^2}\right) p(\mathbf{r}, t)\, dt + \mu \nabla R_{TV}; \tag{8}$$

$$\frac{\partial \varepsilon}{\partial \alpha_0} = \sum_{m=1}^{M} \int_0^T p^*(\mathbf{r}, T-t)\, w(T-t)\left(-2c^{y-1}(-\nabla^2)^{\frac{y}{2}}\frac{\partial}{\partial t} + 2c^y \tan\left(\frac{\pi y}{2}\right)(-\nabla^2)^{\frac{y+1}{2}}\right) p(\mathbf{r}, t) dt + \mu \nabla R_{TV} \tag{9}$$

Here w is a chosen time window and the term $\mu \nabla R_{TV}$ can be calculated numerically. The adjoint field (p^*) that appears in Eq. (8) and Eq. (9) is obtained by solving the Fractional Laplacian wave equation (using k-Wave) with an adjoint source term given by:

$$S^*(r,t) = \sum_{m=1}^{M} [p(\boldsymbol{r}_m, T-t) - p^{obs}(\boldsymbol{r}_m, T-t)]\, w(T-t)\delta(\boldsymbol{r} - \boldsymbol{r}_m)$$
$$+ \beta \sum_{m=1}^{M} \left[\frac{A_m{}^{obs}}{A_m{}^{sim}} - 1\right] p(\boldsymbol{r}_m, T-t)\, w(T-t)\delta(\boldsymbol{r} - \boldsymbol{r}_m) \tag{10}$$

Note the fractional Laplacian term in Eq. (9) becomes simpler to compute in the Fourier domain[12,13]

$$(-\nabla^2)^y p(r,t) = \mathcal{F}^{-1}\{k^{2y}\mathcal{F}[p(r,t)]\}, \tag{11}$$

where $\mathcal{F}$ and $\mathcal{F}^{-1}$ are the forward and inverse Fourier transforms, respectively, and k is the wave number matrix.

2.3 Scheme of the reconstruction and initial models

Using the alternating minimization procedure explained in Sec. 2.2, the scheme of our reconstructions consists on first, obtaining the SS distribution using initial estimates of the SS and AA distributions and after that, the reconstructed SS is employed to recover the AA distribution. In the reconstruction of the SS we set β to cero in Eq. (10) and Eq. (5), and employed only the standard misfit function, as this term is robust enough to perform the SS reconstruction. For the AA reconstruction we set β=10 based on several numerical test where we looked for the fastest decrease of the error functional shown in Eq. (5) along a given number of iterations. The initial estimates for the AA and SS were obtained with a bent-rays algorithm based on the Fast Marching Method (FMM)[20]. This is a fast high-frequency approximation that takes into account the refraction of the wave due to the SS heterogeneities of the medium. The propagation is given by bent lines connecting emitter and receiver pairs. To obtain the FMM-SS image, the first arrival values of the signals were calculated. For the case of the FMM-AA image, the amplitude decay method was employed[21] using the maximum amplitude of the recorded signals relative to its water amplitude.

2.4 Numerical experiments

In order to test the performance of the proposed misfit function, we simulated a numerical phantom with several structures mimicking breast tissue (see Fig. 2 A and C). After the forward simulation, random Gaussian noise was added to the recorded data to give a signal-to-noise ratio (SNR) of 40 dB. This is similar to the SNR achievable with our experimental USCT prototype[22].

The USCT geometry was a ring array of radius 54 mm with N=200 uniformly distributed transducers. The simulations were conducted on a 128 mm×128 mm grid represented by 128×128 grid points with a 10-grid point perfectly-matched layer positioned outside the domain[14]. The transmitted signal was a Gaussian enveloped 3-cycle sinusoidal tone burst with a 500 kHz central frequency. Under these conditions the simulation time for each projection for a single emitter was 0.23 seconds using an Intel Core i7-3930K CPU @ 3.20GHz with an NVIDIA GeForce GTX 780 Ti GPU.

Downloaded From: https://www.spiedigitallibrary.org/conference-proceedings-of-spie on 11/27/2017 Terms of Use: https://www.spiedigitallibrary.org/terms-of-use

To quantify the reconstructions, the mean and standard deviation of the pixel values within several regions of interest (ROIs) located inside the lesions and structures of the numerical phantom were obtained and compared with the expected values in those ROIs (Table 1).

3. RESULTS

The bent-ray initial images employed to initialize the algorithm can be seen in Fig. 2. These images present low resolution and low image quality in general, basically because at these low frequencies the algorithms based on geometrical acoustic provide worst results in comparison with higher frequencies. Edge information for these images is practically lost. Nevertheless, these images provide fast overall information about the region under study.

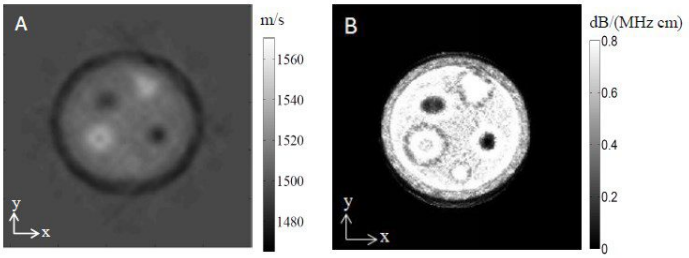

Figure. 2 – A. Initial SS and B. Initial AA reconstructions using a bent-rays algorithm for the numerical phantom shown in Fig. 3A and 3C.

Fig. 3 shows the images reconstructed for the SS using the standard misfit function (Fig. 3 A), and the AA using the standard (Fig. 3 D) and the proposed misfit function (Fig. 3 E). These images were obtained with 10 iterations and a backtracking line search algorithm. As it can be seen comparing figures 3A and 3B, only small deviations from the actual model are obtained for the SS when using the standard misfit function. The major differences appear at the edges of the structures. The larger errors in this case were obtained in ROI 5. On the other hand, the AA reconstruction with the standard misfit shows some artefacts which are significantly removed with the use of the proposed misfit. The results of the quantification of the reconstructed AA images employing both misfit functions are presented in Table 1.

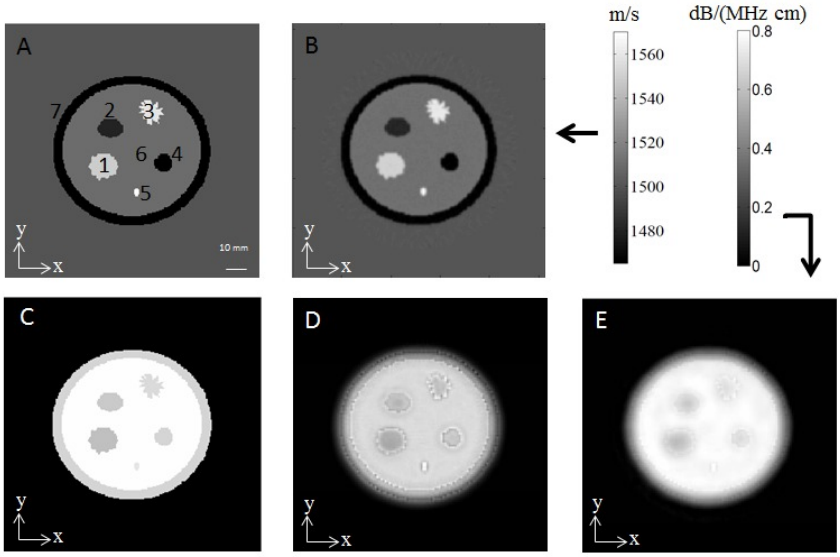

Figure. 3 - A. Reference speed map B. Reconstructed speed map using the standard misfit function. C. Reference attenuation map. D. Reconstructed att. map using the standard misfit function. E. Reconstructed attenuation map using the proposed misfit function.

Downloaded From: https://www.spiedigitallibrary.org/conference-proceedings-of-spie on 11/27/2017 Terms of Use: https://www.spiedigitallibrary.org/terms-of-use

4. DISCUSSION AND CONCLUSIONS

Fig. 3 shows how small differences in the SS map (Fig. 3B with respect to Fig. 3A) create a significant bias in the attenuation map (Fig. 3D with respect to Fig. 3C, and Table 1). The proposed method reduces this bias (Fig. 3E) considerably (Table 1), making it more robust to the deviations in the SS map that normally appear in the reconstruction process. Besides, the region of variation of the bias when using the proposed misfit is smaller than the one obtained with the standard misfit, which is especially remarkable at ROI 5 where the obtained errors in the SS map were larger. This means that our objective to decrease the dependence on the SS map was achieved in a great extent. The improvement still present some dependence on the characteristics of the region evaluated, as the effect of the least squares misfit function is ameliorated but not complete eliminated. Nevertheless a significant overall reduction of the bias without affecting the noise is obtained. The relative weight of both terms in the proposed misfit function is controlled by a parameter β. With $\beta = 0$, we recover the standard method, which is able to obtain high-resolution AA maps when the SS map is perfectly known, but creates significant bias when there are some deviations in the estimated SS map. With $\beta >> 1$, the amplitude misfit function is used, obtaining unbiased, but low-resolution images. With the appropriate value (for instance, β =10 as in the examples of this work) a good trade-off between bias and resolution can be obtained with very little additional computational cost.

Table 1. Mean values and standard deviation for the reconstructed attenuation images

		Least squares misfit function			Proposed misft function		
ROI Number	Expected (dB/MHz^y/cm)	Mean value (dB/MHz^y/cm)	Std. Dev	Bias (%)	Mean value (dB/MHz^y/cm)	Std. Dev.	Bias (%)
1	0.57	0.63	0.05	10.53	0.62	0.03	8.77
2	0.6	0.66	0.02	10.00	0.65	0.02	8.33
3	0.65	0.70	0.05	7.69	0.69	0.02	6.15
4	0.63	0.67	0.04	6.35	0.67	0.02	6.35
5	0.68	0.82	0.06	20.59	0.74	0.01	8.82
6	0.75	0.7400	0.0005	1.33	0.751	0.001	0.13
7	0.63	0.57	0.05	9.52	0.59	0.05	6.35

In this work, we propose a new generalized misfit function for the reconstruction of AA and SS maps in USCT. The proposed misfit function includes a term additional to the standard least squares misfit function making it more sensitive to the differences of amplitude of the signals. The proposed method makes the problem more convex, rendering the convergence of the AA reconstruction more robust against possible deviations in the estimated SS map (which remains fixed during the reconstruction of the AA map). By incorporating also a TV regularization term, we can further reduce the noise and possible artifacts in the image while preserving the information of the edges. We are exploring a further generalization of this approach, including additional terms, based for instance on travel-time differences of the measured and simulated signals. This could further reduce the dependence of the convergence and the final results on the initial estimations of both the speed and attenuation maps, improving the global performance of USCT reconstruction methods.

REFERENCES

[1] Mast, T. D. "Empirical relationships between acoustic parameters in human soft tissues," Acoustics Research Letters Online 2, pp. 37-42 (2000).

[2] Tarantola A. “Inverse Problems Theory, Methods for Data Fitting and Model Parameter Estimation”, Elsevier, Netherlands (1987).

[3] Wang, K., Matthews, T., Anis, F., Li, C., Duric, N. and Anastasio, M. "Waveform inversion with source encoding for breast sound speed reconstruction in ultrasound computed tomography," Ultrasonics, Ferroelectrics, and Frequency Control, IEEE Transactions on 3, pp. 475-493 (2015).

[4] Wiskin, J., Borup, D., Johnson, S., Berggren, M., Abbott, T. and Hanover, R. "Full-wave, non-linear, inverse scattering," in Acoustical Imaging" Full-wave, non-linear, inverse scattering," (Springer), pp. 183-193 (2007).

Downloaded From: https://www.spiedigitallibrary.org/conference-proceedings-of-spie on 11/27/2017 Terms of Use: https://www.spiedigitallibrary.org/terms-of-use

[5] Roy, O., Jovanović, I., Hormati, A., Parhizkar, R. and Vetterli, M. "Sound speed estimation using wave-based ultrasound tomography: theory and GPU implementation," SPIE Medical Imaging, International Society for Optics and Photonics, pp. 76290J-76290J-12 (2010).
[6] Sandhu, G. Y. S., Li, C., Roy, O., West, E., Montgomery, K., Boone, M. and Duric, N. "Frequency-domain ultrasound waveform tomography breast attenuation imaging," SPIE Medical Imaging, International Society for Optics and Photonics, pp. 97900C-97900C-12 (2016).
[7] Pérez-Liva, M., Herraiz, J. L., Udías, J. M., Cox, B. T., & Treeby, B. E., "Full-wave attenuation reconstruction in the time domain for ultrasound computed tomography". In Biomedical Imaging (ISBI) IEEE, pp. 710-713 (2016).
[8] Bozdağ, E., Trampert, J., & Tromp, J. Geophysical Journal International, 185(2), 845-870 (2011).
[9] Tejero, C. J., Dagnino, D., Sallarès, V., and Ranero, C. R. "Comparative study of objective functions to overcome noise and bandwidth limitations in full waveform inversion". Geophysical Journal International, 203(1), pp. 632-645 (2015).
[10] Tromp, J., Tape, C., & Liu, Q. "Seismic tomography, adjoint methods, time reversal and banana-doughnut kernels". Geophysical Journal International, 160(1), 195-216 (2005).
[11] Duck, F. Physical Properties of Tissue: A Comprehensive Reference Book (London: Academic, Harcourt Brace Jovanovich) (1990).
[12] Chen, W. and Holm, S. "Fractional Laplacian time-space models for linear and nonlinear lossy media exhibiting arbitrary frequency power-law dependency," J. Acoust. Soc. Am. 4, 1424-1430 (2004).
[13] Treeby, B. E. and Cox, B. T. "k-Wave: MATLAB toolbox for the simulation and reconstruction of photoacoustic wave fields," J. Biomed. Opt. 2, 021314-021314-12 (2010).
[14] Treeby, B. E. and Cox, B. "Modeling power law absorption and dispersion for acoustic propagation using the fractional Laplacian," J. Acoust. Soc. Am. 5, 2741-2748 (2010).
[15] Treeby, B. E., Jaros, J., Rendell, A. P. and Cox, B. "Modeling nonlinear ultrasound propagation in heterogeneous media with power law absorption using a k-space pseudospectral method," J. Acoust. Soc. Am. 6, pp. 4324-4336 (2012).
[16] Rudin, L. I., Osher, S. and Fatemi, E. "Nonlinear total variation based noise removal algorithms," Physica D 1, pp. 259-268 (1992).
[17] Niesen, U., Shah, D. and Wornell, G. W. "Adaptive alternating minimization algorithms," Information Theory, IEEE Transactions on 3, pp. 1423-1429 (2009).
[18] Snyman, J. Practical mathematical optimization: an introduction to basic optimization theory and classical and new gradient-based algorithms (Springer Science & Business Media Vol. 97), pp. 1-257 (2005)
[19] Norton, S. J. "Iterative inverse scattering algorithms: Methods of computing Frechet derivatives," J. Acoust. Soc. Am. 5, pp. 2653-2660 (1999).
[20] Gómez, J. V., Vale, A., Valente, F., Ferreira, J., Garrido, S., & Moreno, L. Fast marching in motion planning for Rhombic like vehicles operating in ITER. In Robotics and Automation (ICRA), 2013 IEEE International Conference on (pp. 5533-5538). IEEE (2013).
[21] Li, C., Duric, N. and Huang, L. "Comparison of ultrasound attenuation tomography methods for breast imaging," SPIE Medical Imaging, International Society for Optics and Photonics, pp. 692015-692015-9 (2008).
[22] Medina-Valdés, L., Pérez-Liva, M., Camacho, J., Udías, J. M., Herraiz, J. L., & González-Salido, N., "Multi-modal Ultrasound Imaging for Breast Cancer Detection" Physics Procedia, 63, 134-140 (2015).
[23] Pérez-Liva, M., Herraiz, J. L., Udías, J. M.,Miller E., Cox, B. T., & Treeby, B. E., "Full Wave Reconstruction in Time Domain of Attenuation and Speed of Sound in Ultrasound Computed Tomography. The Journal of the Acoustic Society of America, 2017 (In press, accepted Feb.3th 2017).

Downloaded From: https://www.spiedigitallibrary.org/conference-proceedings-of-spie on 11/27/2017 Terms of Use: https://www.spiedigitallibrary.org/terms-of-use